Proceedings of The Institute of Acoustics

ACOUSTIC PROPAGATION, INTERNAL WAVES, AND FINESTRUCTURE

Terry E. Ewart

Applied Physics Laboratory and the School of Oceanography
University of Washington, Seattle, Washington 98105

ABSTRACT

We have progressed in our understanding of wave propagation in random media to the point where theoretical predictions of the fluctuations in sound waves that have passed through a medium with a known autocorrelation function are quite accurate. This paper is a brief review of that progress in the context of ocean acoustic scattering. Analytic predictions from 4^{th} moment theory of the range-depth-time phase and intensity fluctuations are shown to agree well with measurements of the complex amplitude of sound waves that have propagated through ocean regions where the index of refraction statistics are well known. The emphasis is on the requirement to understand fully the statistics of the ocean medium. Models of the acoustic index of refraction correlations that result from oceanic tides, internal waves, and finestructure processes will be discussed. Comparison of measured and predicted acoustic fluctuations will be presented to indicate the level of our understanding. Our knowledge of the scattering processes allows us to consider the problem in an inverse sense. That is, we use the equations of scattering to obtain a stochastic inverse from acoustic data. Examples will be given from the Mid-Ocean Acoustic Transmission Experiment, MATE, of both the forward problem and the inverse problem. Models of the oceanic internal wave, finestructure and tidal processes obtained from the measured acoustic fluctuations, are compared with those measured. A discussion of the future expectations from stochastic inverse analysis will be given.

INTRODUCTION

Our knowledge of wave propagation in random media has advanced significantly in recent years. For the case of sound propagation in the volume of the ocean, a significant step was the recognition by Uscinski (1980,1982) that multiple scattering theory was required to account for the large intensity fluctuations observed at mid-ranges. The measurements used in testing the theory were made during the 1971 Cobb Seamount acoustic transmission experiment. In that experiment 4 and 8 kHz pulsed tones were recorded after traversing an 18 km fixed refracted path (Ewart 1976). Other investigators before and after Uscinski's work invoked the Rytov approximation to explain the Cobb results even though the measured scintillation indices were above one, and the log intensities at 4 and 8 kHz did not exhibit Rytov scaling. This is a testament to the requirement that theory not proceed independently of experiment. Application of multiple scatter 4^{th} moment theory to the intensity fluctuations observed in the Cobb experiment and in MATE (1977), made it clear that two major difficulties remained before theory and experiment could agree. [MATE was carried out at 2,4,8, and 13 kHz in the same location as the Cobb experiment (Ewart and Reynolds 1984)] The first was the lack of precision in our knowledge of the transverse correlation function, TCF, of the ocean. The second arose from the fact that the fourth moment theoretical solutions were evaluated only approximately. See Macaskill (1983) and Uscinski *et al* (1986) for discussion of a more precise evaluation of the basic fourth moment solutions.

In this review I will present an overview of the status of the predictions of the experimental

results. In doing so I will address the the evolution of our knowledge of the transverse correlation function based on internal waves and finestructure. Having demonstrated the evolution of our thinking in the development of realistic ocean models, and showing the rather convincing theory-experiment comparisons, I will give a review of our use of the acoustic data to obtain the ocean correlation function as a stochastic inverse. This inverse method is based on a paper by Uscinski (1986). The forward and the inverse scattering problems are examined using the same data set. I will thus try to link our understanding of the statistics of the fluctuating ocean index of refraction field with our understanding of the fluctuating acoustic field. I will then point out areas where an improved understanding is required, and indicate needed research topics. I will begin with a discussion of the TCF as it is modeled from the processes of internal waves and finestructure.

THE TRANSVERSE OCEAN CORRELATION FUNCTION

In order to predict the variability of acoustic waves propagating in the ocean, we need to know the full space-time correlation function of the medium, $R(\xi, \eta, \zeta, \tau)$, where ξ,η,ζ,τ are the space and time difference coordinates. We consider propagation in the x direction with z as the depth. The index of refraction, n, is usually written as a depth dependent deterministic part and a fluctuating part.

$$n(x, y, z, t) = 1 + \langle n_d(z) \rangle + \langle \mu^2 \rangle^{1/2} n_1(x, y, z, t) \tag{1}$$

Certainly in most ocean cases, $\langle \mu^2 \rangle$ is a function of depth also. In our case we assume cylindrical symmetry, and ignore the y dependence in the correlations. We consider ocean regimes where $\langle \mu^2 \rangle$ can be considered independent of depth (Cobb Seamount at the experiment depth of 1000 m is such a region). Then,

$$R(\xi, \zeta, \tau) = \langle n_1(i)\, n_1(j) \rangle, \tag{2}$$

where the i, j refer to different space-time points. We need a few parameters of the medium to carry the proper normalizations; they are the scattering strength Γ, the scaled range, X, and an integral horizontal scale, L_p, where,

$$\Gamma = k^3 \langle \mu^2 \rangle L_v^2 L_p,$$

$$X = \frac{\text{propagation range}}{k\, L_v^2}, \text{and}$$

$$L_p = \int_{-\infty}^{\infty} R(\xi, 0, 0)\, d\xi\,. \tag{3}$$

L_V is the vertical correlation scale of the index of refraction, and k is the acoustic wavenumber. In general the space-time correlation function of internal waves in the ocean has been taken to be separable in the depth and time coordinates. The normalized TCF function needed as input to theory or numerical experiment is the integral projection of R on a plane transverse to the propagation direction is

$$\rho(\zeta, \tau) = \int_{-\infty}^{\infty} R(\xi, \zeta, \tau)\, d\xi = L_p \frac{\Theta(\zeta)}{\Theta(0)} \frac{\Psi(\tau)}{\Psi(0)}\,, \tag{4}$$

where the assumptions are the standard linear internal wave dispersion relation, and separability

of the depth lag and time lag correlations. (Henceforth, TCF will refer to the normalized form.) This allows us to use any of the separable spectral models of linear internal waves. At this point I will review some ocean experiment specifics before discussing the models of internal waves and finestructure that we use.

As a critical test of theory, the experiment design was to make simultaneous, independent measurements of the environmental and acoustic fluctuations. The space-time sound velocity structure of the transmission path region of MATE was studied using the various sensor systems depicted in Fig. 1. The moored sensors sampled the depth-time temperature, salinity, and current structure with 3 moorings located at the corners of a triangle approximately 350 m on a side. The Self-Propelled Research Vehicle, SPURV, recorded temperature, salinity, and pressure data while depth cycling on trajectories oriented 45 degrees to the vertical along the outer edges of a box 6 km on a side by 100 m depth. This data provides information on the horizontal-vertical spatial correlations. SPURV was also operated on isobaric trajectories to study horizontal isotropy and homogeneity. The CTDSV was used to record temperature, salinity, and pressure in two modes. In the first mode 38 profiles were taken at stations spaced 1/4, 1/2, and 3/4 along the MATE transmission path to obtain the depth-large scale horizontal correlations. In the other mode the CTDSV was depth cycled over 1000-1300 m every 20 min for 25 h. This data provides detailed depth-time correlations. The acoustic raypath spanned a depth range of 1000-1200 m, so our interest is in the index of refraction correlations in that range.

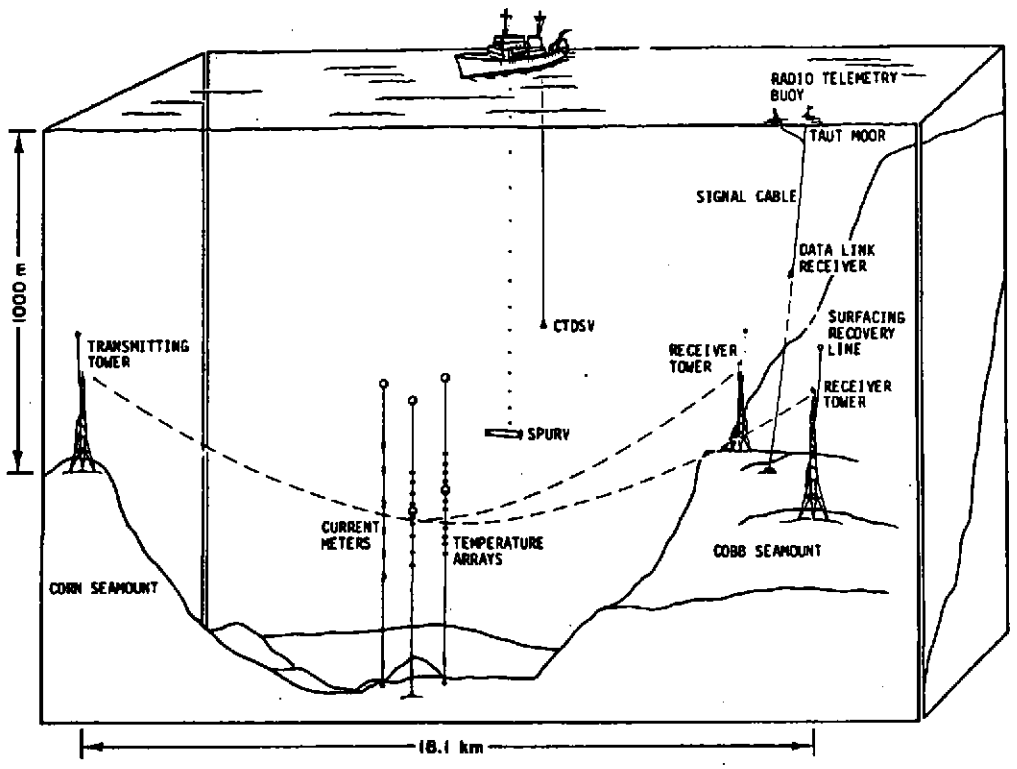

Fig. 1. Layout of the MATE oceanographic and acoustic measurement apparatus.

ACOUSTIC PROPAGATION, INTERNAL WAVES, AND FINESTRUCTURE

The extensive oceanographic and acoustic measurements made during MATE allow us to examine the relationship between the oceanographic variability and the acoustic variability in considerable detail. To give the reader a feeling for the need to obtain the full space-time description of the acoustic index of refraction field, I have included some of the MATE oceanographic results presented in the context of a study of internal waves by Levine *et al* (1986). Earlier work on the so-called finestructure oceanography of MATE is found in Levine and Irish (1981). The results presented in the following figures are given in spectral form, i.e. the Fourier transform of Eq. 2. The transformed variables corresponding to ξ, ζ, τ are α, β, f.

Figure 2 shows the mean sound velocity and buoyancy frequency profiles for the MATE site. The sound velocity is quite linear over the depth range of the transmission path. The buoyancy frequency is nearly constant in the raypath region, and is exponential in depth; this agrees with the standard theoretical formulation of internal gravity waves. Two displacement spectra computed from the 883m and 1273m moored temperature sensors are plotted in Figure 3. The diurnal and semidiurnal tide lines (.042 and .081 cph) stand out at the low frequency end of the internal wave band with only a small inertial frequency peak (.061 cph). The internal wave band shows a rise at the inertial frequency, a falloff to the buoyancy frequency ($\approx$1.0 cph), and a sharp drop at higher frequencies. The moored velocity spectra for the current meter at 1079m is plotted in Fig. 4 showing both the clockwise and the anticlockwise rotary forms. As expected, the clockwise spectrum shows the inertial peak to be the strongest with the diurnal and semidiurnal peaks equivalent in the MS_+ and MS_- spectra. In both figures the Garrett and Munk (1979) form of the linear internal wave prediction is shown as a dashed line with the Levine and Irish form shown as a solid line. The Levine and Irish form will be discussed in more detail subsequently. Figure 5 shows the vertical coherence of the displacement field for temperature sensor separations of 1, 25, and 240 meters.

Determination of the spatial spectrum of the internal wave field was made using data recorded by SPURV and the CTD probe. Figures 6 and 7 show the vertical wavenumber displacement spectra computed from operations of SPURV on isobaric trajectories and data taken with the CTD operated in a yo-yo fashion. In Fig 6. the horizontal wavenumber spectra computed from the north and south trajectories of SPURV indicate isotropy. This provides justification for dropping the y dependence in Eq. 2. The solid line from 4.0×10^{-4} to 10^{-2} cpm is the Levine and Irish theoretical form. The vertical wavenumber spectra plotted in the two curves in Fig. 7 represent estimates computed from the depth ranges indicated.

There are many more projections of the full spectral form that can be derived from the MATE data. See Levine and Irish (1981), Ewart and Reynolds (1984), or Levine *et al* (1986) for thorough discussions. We believe that the data provide an adequate test of linear internal wave models. I will present only the spectral form of the model and the forms of Eqs. 3 and 4 here.

The Levine and Irish spectral model is

$$F(\beta,f) = \sigma^2 \frac{\beta_1\beta_2}{2(\beta_2-\beta_1)\beta^2} \frac{f_I^{1/2} f_N^{1/2}}{4(f_N^{1/2}-f_I^{1/2})f^{3/2}}, \qquad (5)$$

where σ^2 is the internal wave displacement variance, and (β_1, β_2, f_I, and f_N) are the lower and upper vertical wavenumber cutoffs and the inertial and the buoyancy frequencies respectively.

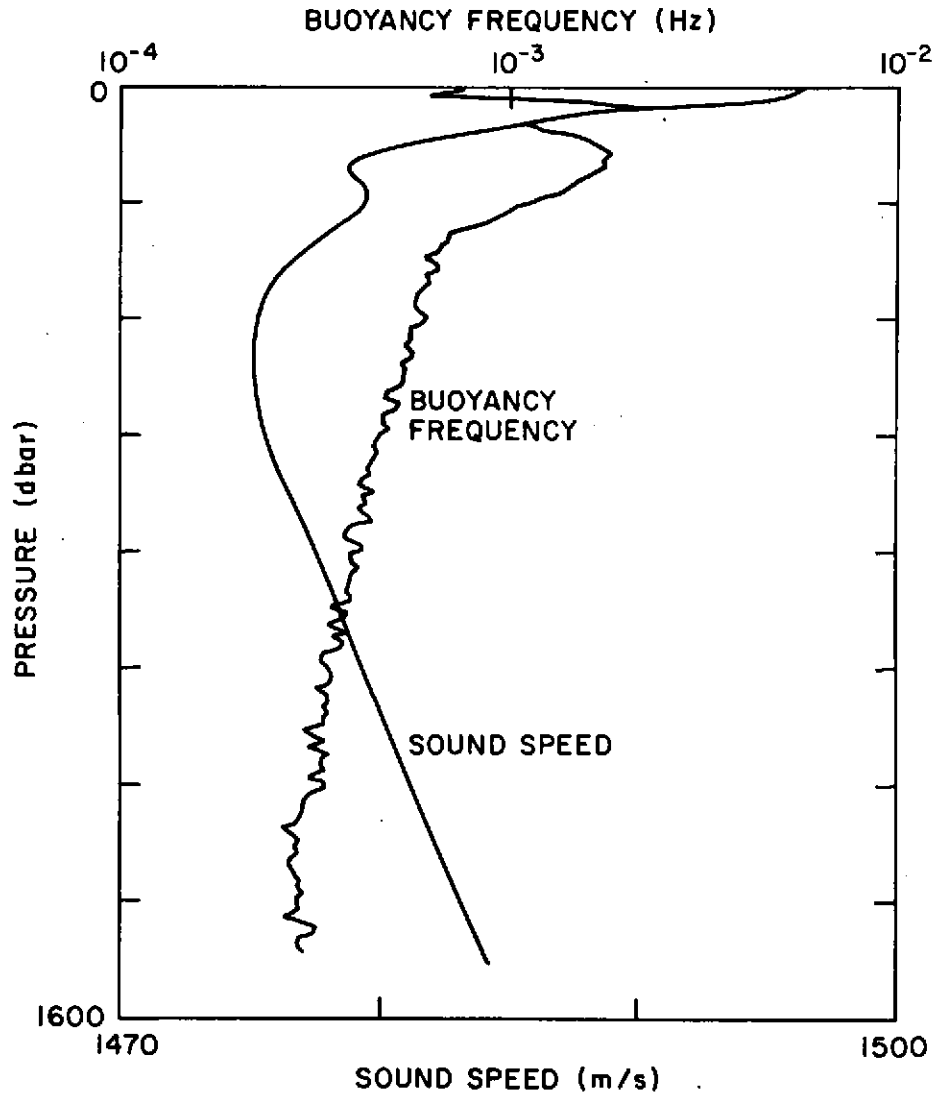

Fig. 2. MATE Sound velocity and Buoyancy Frequency profiles.

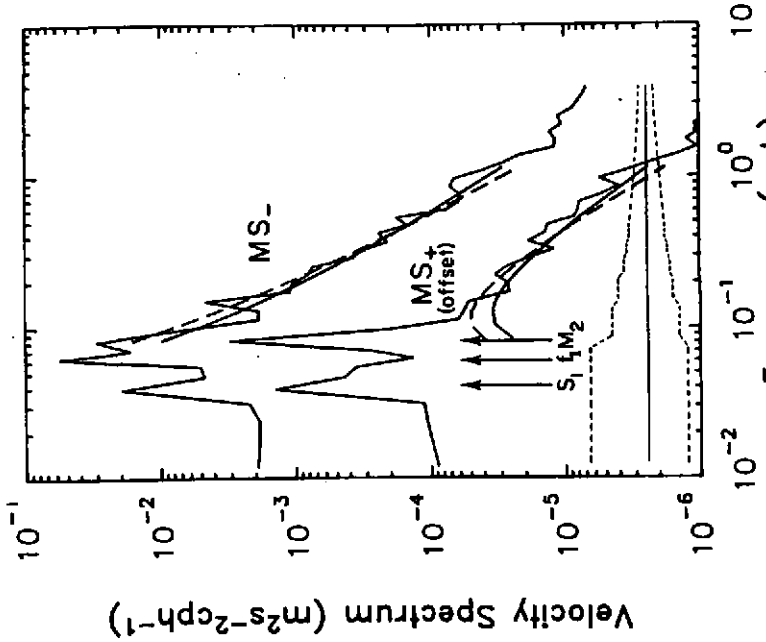

Fig. 4. Rotary velocity spectra (Diurnal, S_1, Semidiurnal, M_2, and Inertial, f_I frequencies shown).

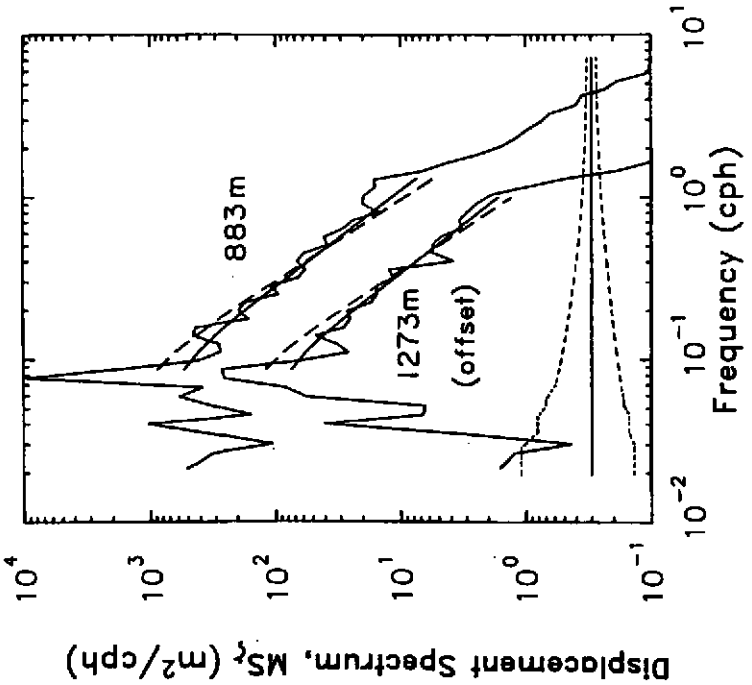

Fig. 3. Displacement spectra from temperature mooring 2.

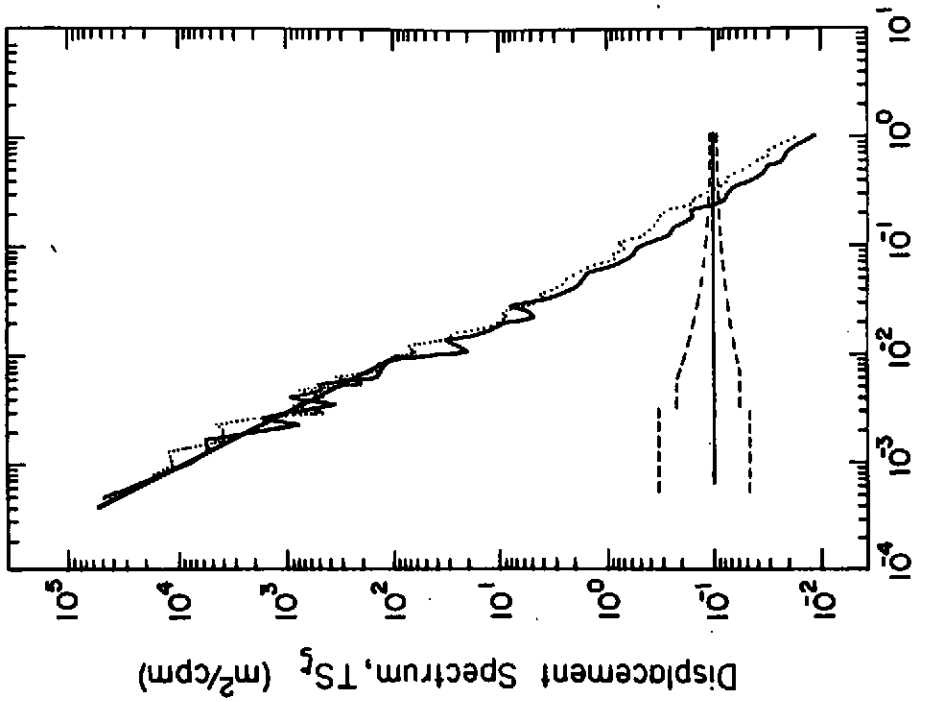

Fig. 6. Displacement spectrum as a function of α.

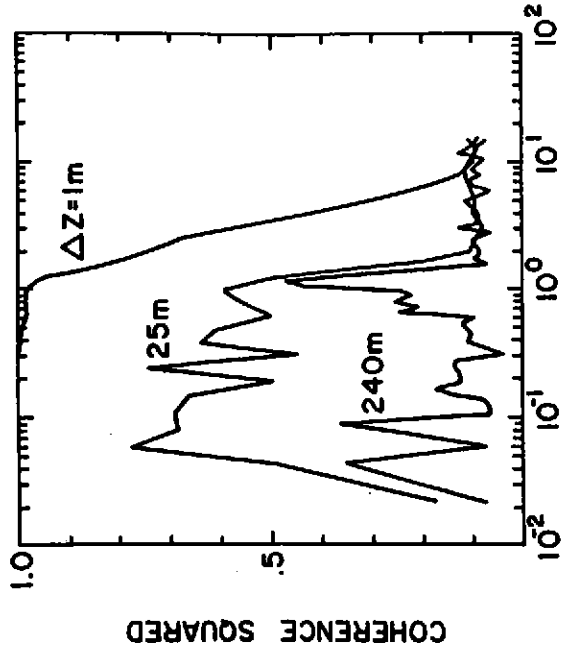

Fig. 5. Moored vertical coherence of displacement for 1, 25, and 240 m separations.

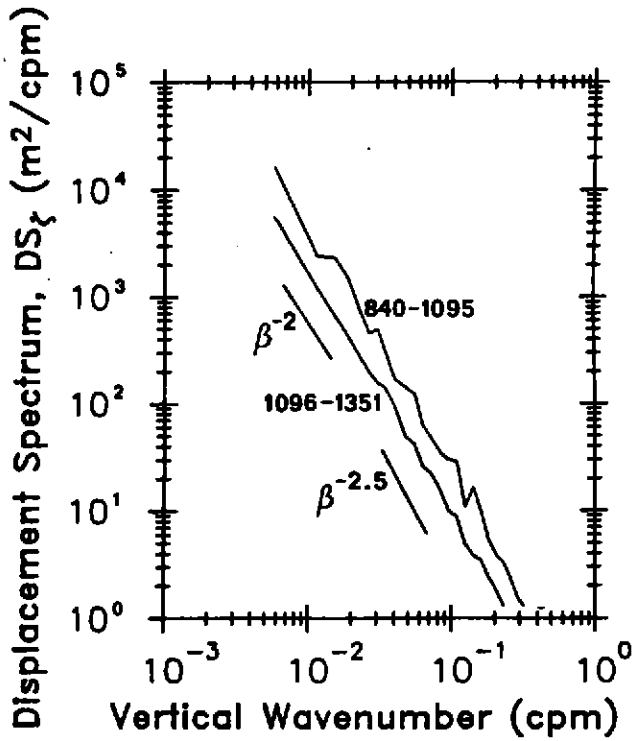

Fig. 7. Displacement spectrum as a function of β.

The integral scale, L_p, and the TCF derived from the internal wave model are,

$$L_p = \frac{\frac{f_N}{\pi}\int_{\beta_1}^{\beta_2}\frac{d\beta}{\beta^3}}{\int_{\beta_1}^{\beta_2}\frac{d\beta}{\beta^2}}\;\frac{\int_{f_I}^{f_N}\frac{df}{f^{3/2}(f^2-f_I^2)^{1/2}}}{\int_{f_I}^{f_N}\frac{df}{f^{3/2}}} \tag{6}$$

$$\rho_{IW}(\delta z,\delta t) = \frac{L_p\;\frac{f_N}{\pi}\int_{\beta_1}^{\beta_2}\frac{\cos(2\pi\beta\delta z)}{\beta^3}\,d\beta}{\int_{\beta_1}^{\beta_2}\frac{d\beta}{\beta^2}}\;\frac{\int_{f_I}^{f_N}\frac{\cos(2\pi f\,\delta t)}{f^{3/2}(f^2-f_I^2)^{1/2}}\,df}{\int_{f_I}^{f_N}\frac{df}{f^{3/2}}}. \tag{7}$$

Equations 6 and 7 are left in integral form; in practice the integrals are done numerically. The extra terms compared to Eq. 5 arise from the dispersion relation. The MATE data appears to support $f^{-1.7}$ in the denominator as opposed to the Levine and Irish model form of $f^{-3/2}$; we have shown this to be an insignificant difference for the 4^{th} moment comparisons. See Ewart and Reynolds (1984). The values of the lower and upper wavenumber cutoffs for MATE are $\beta_1 = 6.9\times10^{-4}m$ and $\beta_2 = 0.1m$ respectively; the inertial frequency, f_I, is 1.66×10^{-5} Hz, and the buoyancy frequency is given by

$$7.34\times10^{-4}\, e^{-\frac{depth}{1309}}\ \text{Hz}. \tag{8}$$

One difficulty in fitting linear internal wave models to the MATE oceanographic data set is the fact that only half of the displacement variance in the vertical wavenumber spectra can be explained by the standard models. The remaining variance has been termed finestructure, and is basically that component of the fluctuations without a wavelike dispersion relationship. The origin of finestructure is uncertain, and many mechanisms have been postulated. As we shall see subsequently, finestructure had to be included with linear internal waves before theoretical predictions of the acoustic intensity fluctuations measured during MATE were in substantial agreement. We have chosen to use a form for the finestructure correlations that is separable and includes the vertical and horizontal coordinate lags and the time lags. We expand on the form given by Levine and Irish (1981), and write the correlation function of finestructure as

$$R_{FS}(\xi, \zeta, \tau) = e^{-\left[\frac{\zeta^2}{L'^2_V} + \frac{\xi^2}{L'^2_H}\right]^{1/2}} e^{-\left[\frac{\tau}{\tau_0}\right]}. \tag{9}$$

The assumptions are that the vertical correlation scale of finestructure is larger than the internal wave displacement. This is supported by observation in the MATE region. This means that the finestructure statistics can be considered independent of those of internal waves. The correlations due to internal waves are controlled by the dispersion relation; we assume that finestructure does not obey a dispersion relation and that the correlations are separable. The spectral form of Eq. 9 is

$$F_{FS}(\alpha, \beta, f) = \frac{1}{\pi\, \alpha_0\, \beta_0\, f_0} \frac{1}{\left[1 + \frac{\alpha^2}{\alpha_0^2} + \frac{\beta^2}{\beta_0^2}\right]^{3/2}} \frac{1}{\left[1 + \frac{f^2}{f_0^2}\right]}, \text{ where}$$

$$\alpha_0 = (2\pi L'_H)^{-1},\ \beta_0 = (2\pi L'_V)^{-1}, \text{ and } f_0 = (2\pi\tau_0)^{-1}, \text{ and} \tag{10}$$

the primes differentiate between internal waves and finestructure. The TCF for finestructure from Eqs. 4 and 9 is,

$$\rho_{FS}(\zeta, \tau) = 2\, \frac{\zeta}{L'_V}\, L'_H\, K_1\!\left(\frac{\zeta}{L'_V}\right) e^{-\left(\frac{\tau}{\tau_0}\right)}, \tag{11}$$

where K_1 is the K_1 Bessel function. Note that,

$$\lim_{\zeta\to 0}\left[2\frac{\zeta}{L'_V} L'_H K_1\!\left(\frac{\zeta}{L'_V}\right)\right] = 0, \tag{12}$$

and if we set $L'_P = 2L'_H$, then

$$\rho_{FS}(\zeta, \tau) = L'_P \frac{\zeta}{L'_V} K_1\!\left(\frac{\zeta}{L'_V}\right) e^{-\left(\frac{\tau}{\tau_0}\right)}. \tag{13}$$

The assumption that $L'_P = 2L'_H$ remains to be verified for finestructure; $L_P \approx 2L_H$ for internal waves. The chosen spectral models for internal waves and finestructure provide the required ζ, τ dependence, and these forms are well fit by the measured oceanographic data. The inclusion of

the time dependence is required in the stochastic formulation. As we will see in the section on the inverse method, the value of τ_0 for finestructure is longer than the longest internal wave period. Physically, it indicates the slow decay of the non wave-like processes. Levine (1979) referred to this as "melted" finestructure, as opposed to the high wavenumber finestructure which is considered to be passive and "frozen". The value of $<\mu^2>$ associated with the "frozen" finestructure is two orders of magnitude below that of internal waves or "melted" finestructure. Hence, we have ignored it for the purposes of acoustic fluctuation predictions. See Ewart *et al* (1983).

It is now possible to write the combination of internal waves and finestructure as L_P times the internal wave TCF plus L'_P times the finestructure TCF. This form can be conveniently used as input to the theoretical solutions of the fourth moment equation to predict the MATE acoustic intensity correlations. We now direct our attention to comparisons of the measured and predicted intensity fluctuations.

EXPERIMENTS COMPARED WITH THEORY - THE FORWARD PROBLEM

It is not my intent to present a summary of the theory, but rather to show the evolution of our success at predicting the MATE fluctuations. I will concentrate in this section on the intensity correlations of the scattered field, because predictions of the lower order moments compare well with measurements. If one examines the predictions of 4^{th} moment theory when multiple scattering effects are not included, they seriously disagree with observations. See e.g. Desaubies (1978), Flatte (1983). Multiple scatter theory is discussed extensively by Uscinski in another section of this conference, and I will present only the results of predictions based on the oceanographic review in the previous section without a review of the theory. The reader is encouraged to examine the experiment-theory comparisons in more detail in Ewart *et al* (1983), Ewart and Reynolds (1984), Ewart *et al* (1985), and Uscinski and Ewart (1986).

I will discuss here the multiple scatter predictions of the 2, 4, 8, and 13 kHz MATE intensity autospectra. The approach we use in the comparisons is to use the experimentally determined values of $\Gamma, X, L_V, L_P, L'_V, L'_P, \beta_1, \beta_2, f_I$, and f_N together with the analytic forms of the TCF's. The theory has evolved in two incarnations. The first, Uscinski *et al* (1983) is termed a "zeroeth" order evaluation of an "exact" integral form. The second, Macaskill (1983), and Uscinski *et al* (1986), includes a correction to the zeroeth order evaluation, and has been termed a "first order" evaluation. I will refer to these solutions as $m_{IV}^{(0)}$ and $m_{IV}^{(1)}$.

The MATE intensity autospectra, $\Phi_{I/<I>}(f)$ are plotted in Fig. 8 with 4, 8, and 13 kHz offset from 2 kHz by successive decades. Four different theoretical predictions are shown based on $m_{IV}^{(0)}$. The predictions differ only in the form of Eq. 5 used to obtain the TCF. The four models are indicated on the figure with differing values of P, where $f^{-(P-1)}$ is the form of the time frequency spectrum. The symbol "LI" refers to the model presented in the previous section, "De" refers to the Desaubies (1976) and "GM" refers to the Garrett and Munk (1979) models. The predictions have approximately the correct spectral form, but the scintillation indices (integral of the normalized intensity autospectra), S_I^2, fall short in all cases. Predictions based on the full internal wave and finestructure models, Eqs. 7 and 13 are shown in Figure 9. The differences in the experimental curves plotted in Figs. 8 and 9 is due to differing techniques of spectral estimation for $f < f_I$. The $m_{IV}^{(0)}$ prediction in Fig. 9 is an improvement over the prediction for internal

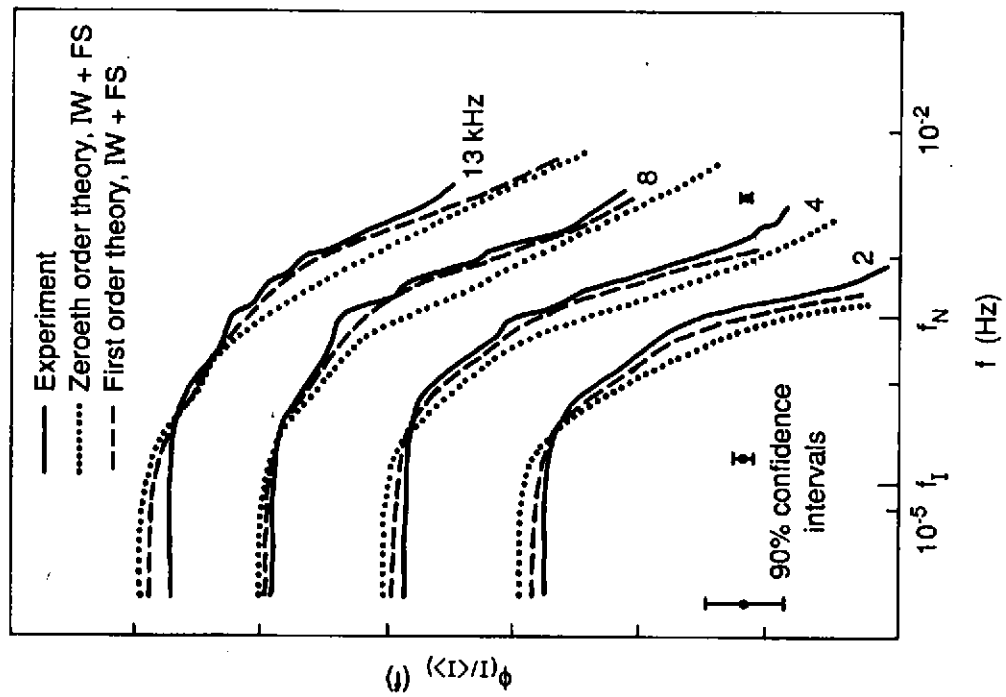

Fig. 9. MATE intensity autospectra plotted with $m_{jv}^{(0)}$ and $m_{jv}^{(1)}$ theory using the combined internal wave and finestructure model.

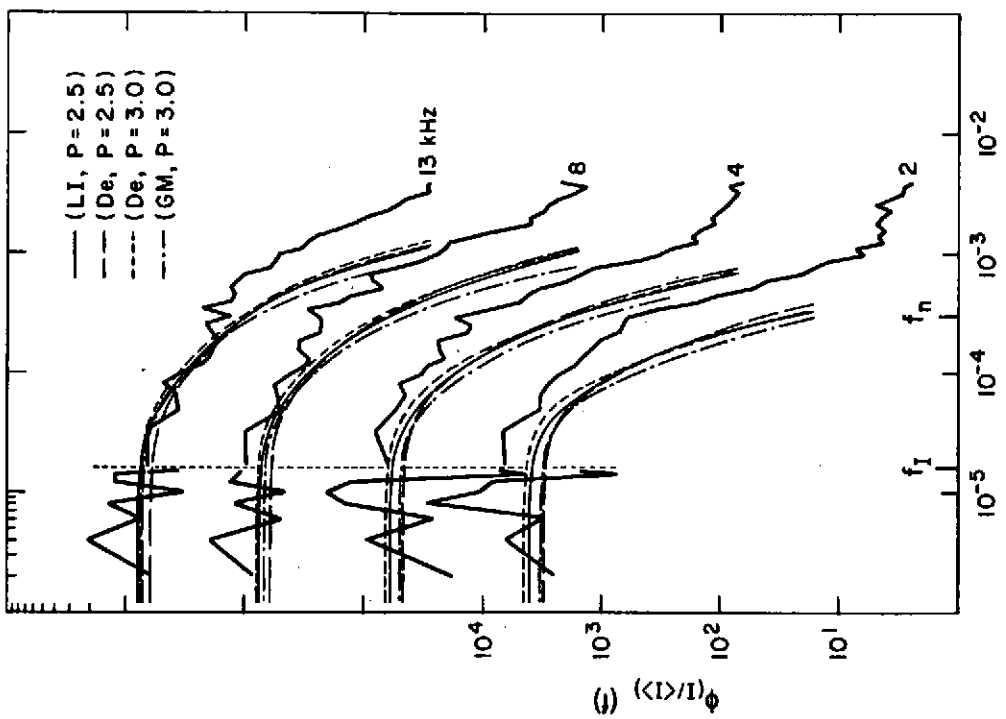

Fig. 8. MATE intensity autospectra plotted with $m_{jv}^{(0)}$ theory using four different models of linear internal waves.

waves only, but the $m_{IV}^{(1)}$ predictions are very close to the experimental curve. Table 1 is a compilation of S_I^2 for the three predictions.

Table 1. MATE Predicted and Measured Scintillation Indices

Freq.	$m_{IV}^{(0)}$ - IW	$m_{IV}^{(0)}$ - IW and FS	$m_{IV}^{(1)}$ - IW and FS	MATE
2.083 kHz	0.26	0.56	0.69	0.73
4.167 "	0.51	0.83	1.21	1.18
8.333 "	0.88	1.17	1.75	1.95
12.5 "	1.09	1.27	1.80	1.85

Comparison of columns 3 and 4 of Table 1 indicates quite good agreement. One of the difficulties in inferring too much from this success is the nature of the multiple scattering process. When ΓX is well above one as it is for most ocean scattering conditions, the acoustic field "forgets" the oceanic field as it propagates. The form of the scattering is thus dominated more by the value of ΓX than it is by the detailed form of the correlation function. This indicates that we need to concentrate more on the lower moments of the acoustic field before we can be certain of the analytic forms of the TCF. Clearly, both internal waves and finestructure models must be included. It is clear from Eq. 4 that the vertical correlations of the index of refraction are equally important. Lacking data on the depth dependence of the acoustic field, we have used numerical techniques to test the z dependence in the 4^{th} moment predictions.

The multiple scattering theory discussed above predicts $\Phi_{I/<I>}(\zeta, f)$. In addition to the agreement of multiple scattering theory with ocean experiment results, the robust nature of the predictions is also evident from tests of the theory with numerical experiments. Macaskill and Ewart (1984) applied numerical parabolic equation methods to test the ζ dependence of the theories. In that work the statistical ocean behavior is simulated with Monte-Carlo methods, and the wavefield is propagated through the simulated environment using the split-step method of Tappert and Hardin (1974). The output is many realizations of the wavefield in transverse coordinate and range for given values of Γ, X, and the TCF. From this numerical data $\Phi_{I/<I>}(\zeta)$ was estimated. The agreement of theory with the numerical experiment results is very good. See Macaskill and Ewart and Uscinski *et al* (1986).

Thus, 4^{th} moment theory and experiment are in accord for wave propagation in random media where the parabolic approximation holds. The large values of Γ, X appropriate to the ocean indicate that multiple scatter theory must be used. This implies an inability to confirm specific models of the TCF, and we sought other methods of testing. In the next section I address preliminary results from a method that uses the measured acoustic fields of MATE to test the ocean models of tides, internal waves and finestructure.

PROGRESS ON THE STOCHASTIC INVERSE PROBLEM

Uscinski (1986) provides a theoretical basis for comparing ocean models with the measured phase and complex amplitude correlations. I will only summarize the theory for the phase correlations, and present some preliminary results obtained from the MATE acoustic data. Uscinski (1977) gives an expression for the two-point phase correlations of a wave propagating in a random

media. In the notation used here, the predicted phase correlations as a function of ζ, and, τ are written

$$R_\phi(\zeta,\tau) = \Gamma X \left[\frac{\theta_{IW}(\zeta)}{\theta_{IW}(0)} \frac{\psi_{IW}(\tau)}{\psi_{IW}(0)} + b \frac{\theta_{FS}(\zeta)}{\theta_{FS}(0)} \frac{\psi_{FS}(\tau)}{\psi_{FS}(0)} \right], \tag{14}$$

$$\text{where } b = \frac{<\mu_{FS}^2>}{<\mu_{IW}^2>} \frac{L'_p}{L_p} \tag{15}$$

gives the ratio of the contributions of internal waves to those of finestructure in the variance of acoustic refractive index fluctuations. The space-time autocorrelation function of the complex acoustic amplitude measured at two receivers is given by the solution of the parabolic second moment equation. Its use in an inverse sense is written by Uscinski in a similar fashion. In the case of the phase and complex amplitude correlations it is necessary to consider the effects of the tides as well as internal waves and finestructure. As the MATE acoustics data was measured as a time series, I will drop the ζ dependence in what follows.

Uscinski assumes a simple harmonic tide, and shows that the tides can be included in Eq. 14 as

$$\frac{R_\phi(\tau)}{k^2} = \frac{\Gamma X}{k^2} \left[\frac{\psi_{IW}(\tau)}{\psi_{IW}(0)} + b \frac{\psi_{FS}(\tau)}{\psi_{FS}(0)} \right] + \frac{A_{SD}^2}{2} \cos\left(2\pi \frac{\tau}{\tau_{SD}}\right) + \frac{A_D^2}{2} \cos\left(2\pi \frac{\tau}{\tau_D}\right), \tag{16}$$

where SD and D refer to the semidiurnal and diurnal tides. The inverse is computed by solving the minimization problem

$$\underset{\Gamma X, b, A_{SD}, A_D}{\text{minimize}} \left[\hat{R}_\phi(\tau) - R_\phi(\tau) \right]^2, \tag{17}$$

where $\hat{R}_\phi(\tau)$ is the measured phase correlation function. The advantage of dividing the equation by k^2 is that the acoustic frequency dependence is removed to first order. The result of solving Eq. 17 for the parameters of $R_\phi(\tau)$ using the MATE 2 kHz phase data is shown in Figure 10. The minimization was carried out using a technique discussed in Sorensen (1982). The internal wave and finestructure models used were Eqs. 7 and 13 with ζ set to zero. The value of τ_0 corresponding to the minimum residual (27h) was found by solving the problem in Eq. 17 for many fixed values. A plot of the individual correlation functions in Figure 11 shows the relationship between the various functional forms. Different expressions for $\psi_{IW}(\tau)$ were tried with little differences in the residuals. The inverse using only time measurements is limited. For those readers familiar with ocean internal wave studies, we canot obtain the energy and bandwidth parameters using $\psi_{IW}(\tau)$ alone. The parameters (e.g. E and j^* in the Garrett and Munk formulation) arise in combination in ΓX. Both time and depth measurements of the acoustic field are required to obtain the parameters independently.

The results are encouraging in that the values of ΓX and b from the minimization are reasonably close to those observed (9.6 versus 14, and 1.1 versus 1.0). The ratio of the semidiurnal tide amplitude to that of the diurnal tide is close to the ratio reported in Larson and Irish (1975) for tides in the Cobb Seamount region. (The method gives only the amplitudes of the tidal current components along the acoustic ray.)

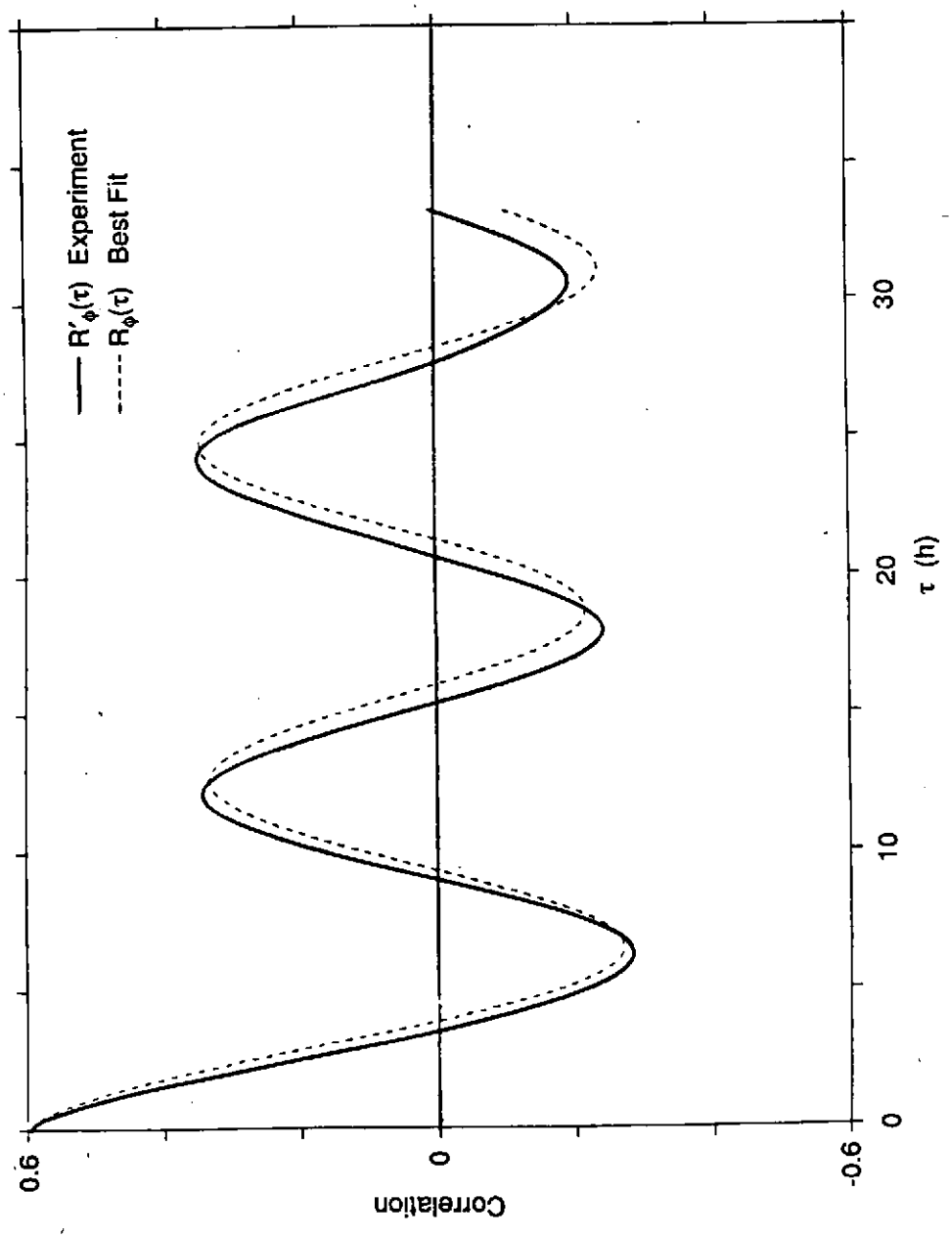

Fig. 10. $\hat{R}_\phi(\tau)$ and $R_\phi(\tau)$ obtained by solving Eq. 17.

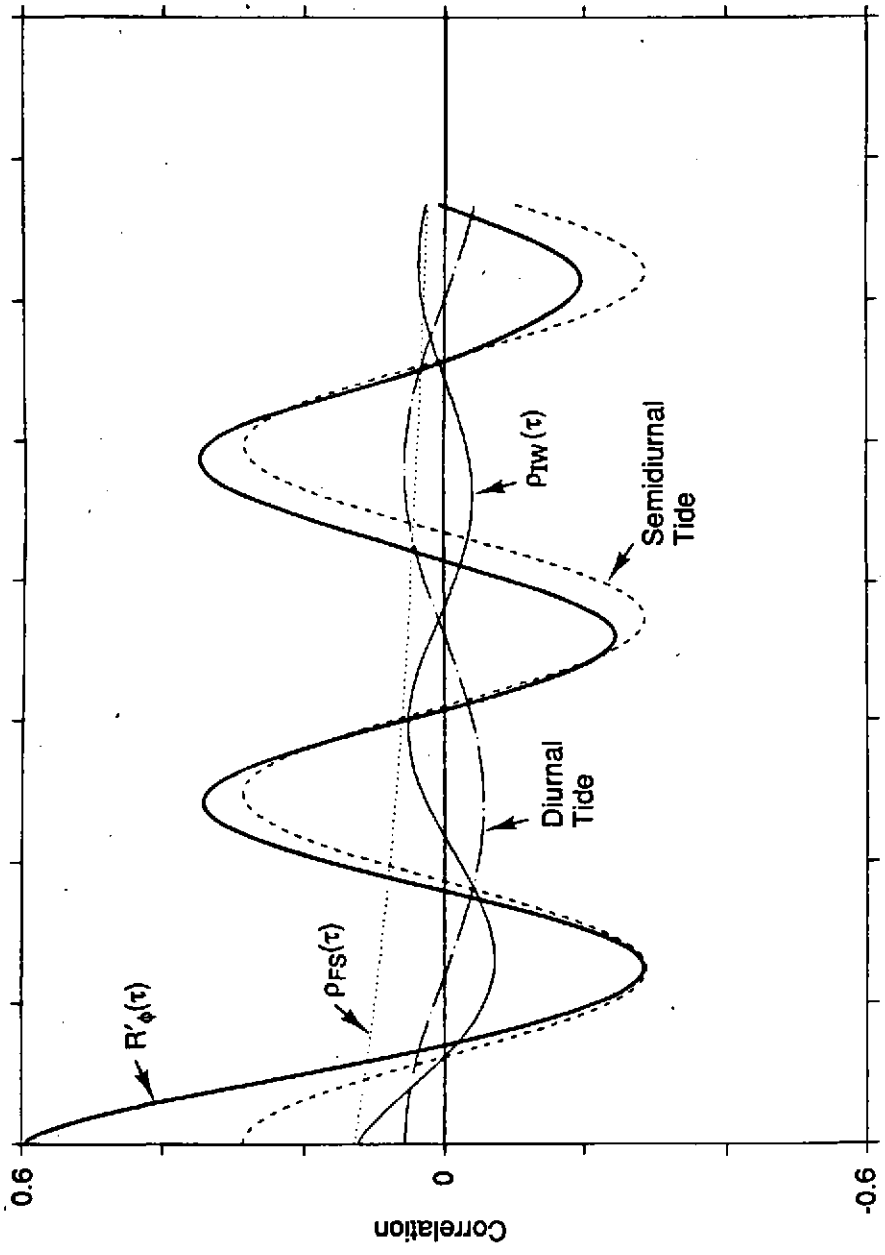

Fig. 11. $\hat{R}_\phi(\tau)$ plotted with the elemental functions of $R_\phi(\tau)$.

The difficulty in obtaining the inverse using the correlation functions arises from the fact that the estimates of the correlation function at different lags are themselves correlated. Because of the oscillatory nature of the tidal and internal wave correlations, there is not an objective criteria for choosing how many lags to use in the inverse. If one wishes to use a weighted minimization technique, it is difficult to assign the weights in view of the fact that the errors in the estimates are also correlated. These problems can be alleviated by reformulating the problem in the frequency domain where the spectral estimates are uncorrelated. This has been completed, and early results are encouraging.

SUMMARY

I have tried to give the reader a feeling for the complexity of the problem one faces when trying to reconcile acoustic scattering theory with experiment. Ultimately, a clearer picture of the oceanography-acoustic relationship will emerge when the forward and inverse methods have been utilized fully. Oceanographers, for their part, are making the world more complex by introducing non-separable internal wave models. In our work so far, we have ignored the mean sound speed profile. Curving raypaths modify the effective TCF due to the angle of the wavefront to the layered ocean statistics. Ray effects are negligible at MATE because of the shallow ray angle and the linear sound speed profile. This is not true for most ocean acoustic scattering conditions. Both the 4^{th} moment theory and the inverse theory will require modification to include those effects.

It is clear that we need to utilize data sets such as MATE to test the ocean models to the extent possible. The MATE acoustics data was recorded for only a single separation in the vertical and a single separation in the horizontal. Before we can use Eq. 16 and its counterpart for the complex amplitude correlations fully, we need to have a data set where the $\hat{R}_{\phi}(\zeta, \tau)$ can be obtained over wide ranges of ζ and τ. Such data will be provided by the 1985 AIWEX Acoustic Transmission Experiment where simultaneous oceanographic and acoustic measurements were made in the Beaufort sea. Ray effects will have to be considered in that case.

We have come a long way from the use of homogeneous isotropic turbulence to model the ocean medium. The lesson learned is that understanding the processes of acoustic scattering cannot proceed without a thorough understanding of the medium. This gives a strong indication of the need to conduct oceanic scattering experiments simultaneously with a complete space-time sampling of the oceanography. Success in the use of stochastic inverse methods indicates that the converse may also be true.

ACKNOWLEDGEMENTS

I would like to thank Drs. Steve Reynolds and Eric D'Asaro for reading the manuscript, Dr Murray Levine for providing me with some of the figures, and the conference conveners for the invitation. This work was supported by the Office of Naval Research Codes 1125UA and 1125AR.

REFERENCES

Desaubies, Y.J.F., J. Phys. Oceanogr. **6** pp976-981 (1976).

Desaubies, Y.J.F., J. Acoust. Soc. Am. **64**, 1460 (1978).

Ewart, T.E., J. Acoust. Soc. Am. **60**, 46 (1976).

Ewart, T., Macaskill, C., and Uscinski, B., J. Acoust. Soc. Am. **74**, (5) pp1484-1499 (1983).

Ewart, T.E. and Reynolds, S.A., J. Acoust. Soc. Am. **75**, 785 (1984).

Flatte, S.M., Proc. IEEE **71** (11) (1983).

Garrett, C. and W. Munk, Ann. Rev. Fluid Mech.- Vol 11, Edited by M. Van Dyke and J.V. Wehausen, pp339-369 (1979).

Larson, L.H., and J.D. Irish, J. Geophy. Res. **80** (12) (1975).

Levine, M.D., Ph.D. Dissertation, Univ. of Washington, Seattle, 172p (1979).

Levine, M.D., and Irish, J.D., J. Phys. Oceanogr. **11**, 676 (1981).

Levine, M., J. Irish, T. Ewart, and S. Reynolds, J. Geophys. Res. **91** (C8) pp9709-9719 (1986).

Macaskill, C., Proc. Roy. Soc. **386**, 461 (1983).

Sorensen, D.C., SIAM J. Numer. Anal. **19** (2) pp409-426 (1982).

Tappert, F.D. and Hardin, R.H., "Proc. 8th Intl. Congress on Acoustics" - Vol. II, p452, London: Goldcrest (1974)

Uscinski, B.J. "The Elements of Wave Propagation in Random Media," New York: McGraw-Hill (1977).

Uscinski, B.J., J. Acoust. Soc. Am. **64** pp1460-1469 (1980).

Uscinski, B.J., Proc. Roy. Soc. **380**, 137 (1982).

Uscinski, B.J., Macaskill, C., and Ewart, T.E., J. Acoust. Soc. Am. **74**, (5) pp1474-1483, 1983.

Uscinski, B., C. Macaskill, and M. Spivack, J. Sound and Vib. **106** (3) 509-528 (1986).

Uscinski, B. J., J. Acoust. Soc. Am. **79** (2)347-355 (1986).

Uscinski, B.J. and T.E. Ewart, Unpublished Manuscript (1986).